A Comparison of Multirate Robust Track-Following Control Synthesis Techniques for Dual-Stage and Multi-Sensing Servo Systems in Hard Disk Drives *

Xinghui Huang, Ryozo Nagamune, and Roberto Horowitz†

September 27, 2005

Abstract

This paper presents the system modelling, design and analysis of multirate robust track-following controllers for a dual-stage servo system with a MEMS microactuator (MA) and an instrumented suspension. A generalized model is constructed which includes a nominal plant, disturbances, uncertainties, and multirate sensing and control. Two major categories of controller design methodologies are considered. The first includes synthesis methodologies that are based on single-input single-output (SISO) design techniques, and includes the sensitivity decoupling (SD) and the PQ methods. In this case, a high sampling-rate inner loop damping control is first implemented using the auxiliary sensor signals. Subsequently, a low-rate outer loop controller is designed for the damped plant using either the SD or PD design methods. The second category of design methodologies includes those based on multirate, multi-input multi-output (MIMO) design techniques, including mixed H_2/H_∞, mixed H_2/μ, and robust H_2 synthesis. In this case, a set of controllers, which is periodically time-varying due to multirateness, is designed by explicitly considering plant uncertainty and hence robust stability. Comparisons are made between all the design techniques in terms of nominal H_2 performance, robust stability, and robust performance between these controllers, when the feedback controller is closed around the full order, perturbed plant. The advantages and disadvantages of each of these methods are discussed, as well as guidelines for their practical implementation.

1 Introduction

Since the first hard disk drive (HDD) was invented in the 1950s by IBM, their storage density has been following Moore's law, doubling roughly every 18 months. Current storage density is about 230 giga-bit per square inch, as reported by Hitachi GST [1].

*This work was supported by the Information Storage Industry Consortium (INSIC), the Swedish Research Council (VR), and the Computer Mechanics Laboratory (CML) of UC Berkeley.

†The authors are with the Department of Mechanical Engineering, University of California, Berkeley, CA 94720 {xhhuang, ryozo, horowitz}@me.berkeley.edu.

A current goal of the magnetic disk drive industry is to surpass the storage density barrier of 1 terra-bit per square inch. It is expected that the corresponding track density for this storage density will be about 500,000 track-per-inch (TPI), requiring a track mis-registration (TMR) budget of less than 5 nm (3σ). To achieve this goal, higher control bandwidth is necessary to attain sufficient positioning accuracy. However, it is difficult to design high bandwidth controllers using only one actuator, the voice coil motor (VCM), due to the presence of suspension resonance modes and hence airflow excited suspension vibrations. A new class of dual-stage actuators for HDDs has been proposed to overcome this problem: a microactuator (MA) is placed at the end of the suspension and moves the slider/head relative to the suspension tip, allowing increased servo bandwidth [2][3].

However, as servo bandwidth is expanded and the desired TMR budget becomes even smaller, the slider motion due to airflow excited suspension vibration becomes more important as the disk rotation speed increases. Since airflow excited suspension vibration is located in a frequency range that is higher than the expected servo bandwidth of dual-stage systems, it cannot be effectively compensated by the servo loop and actually may even be amplified. Suspension vibration control schemes using instrumented suspensions along with dual-stage servo systems have thus been proposed. The sensor output from instrumented suspensions can be utilized for vibration mode damping by the VCM [4], or be used for feedforward vibration compensation by the MA [5], or both [6].

Several controller design methods have been proposed for MEMS-based dual-stage servo systems, which can be roughly categorized into two major groups. The first group includes those methodologies that utilize sequential SISO frequency shaping design techniques, such as the PQ method [7] and the sensitivity decoupling (SD) method [8]. These methods are straightforward to understand and utilize mature SISO design techniques. Stability robustness is taken care of by gain and phase margins, which are obviously inadequate for MIMO systems. The inherent coupling property of the plant cannot not be fully exploited with these techniques, which usually yields a closed-loop system with conservative performance and also poor robustness performance properties. On the other hand, the designed controller is usually of low order and therefore easy to implement.

The second group includes multi-variable optimal control design techniques such as μ-synthesis [9] and mixed H_2/H_∞ [6]. With the use of a state-space model, these methods can systematically take into account coupling dynamics and plant uncertainty during the design process. The nominal system's performance can therefore be optimized while still retaining robust stability with respect to modelled uncertainty. The designed controller usually has a higher order than that of their SISO counterparts, even after controller order reduction. Therefore, a careful tradeoff is always necessary when considering computation power, implementation reliability, and achievable performance.

In a MEMS-based dual-stage system with an instrumented suspension, the strain sensor signal and the relative motion information from the MA's capacitive sensor can be sampled at a higher rate than that of the position error signal (PES). The scheme of multirate sensing and multirate control can then be incorporated into the controller design, either in sequential SISO or MIMO techniques. Multirateness can be incorporated into SISO design techniques by using high-rate inner loop controllers followed by a low-rate outer

loop controller. While in MIMO design techniques, it can be incorporated into a single MIMO controller designed based on an auxiliary frequency-lifted, time-invariant system [10]. With high-rate sensing, better performance can be expected for track following and vibration attenuation.

This paper presents the system modelling, design and analysis of robust track-following controllers for a dual-stage servo system with a translational MEMS MA and an instrumented suspension. In Section 2, a generalized model is built, which includes all frequency-shaped disturbances, uncertainties, multirate sampling and control. Section 3 introduces various multirate robust design approaches, including SISO and MIMO design techniques. Design and simulation results are presented in Section 4.

2 A General Model for a Dual-Stage Assembly with a MEMS Microactuator and an Instrumented Suspension

2.1 The Nominal Plant

The structure of the dual-stage actuator with an MA and a strain sensor is illustrated in Fig. 1 and its block diagram is shown in Fig. 2. In Fig. 2, G_V and G_M represent the dynamics of the VCM and MA respectively. u_v and u_m are the control inputs, and $\mathrm{w_v}$ and $\mathrm{w_m}$ are the airflow disturbances to VCM and MA respectively. y_h, y_p, y_m are respectively the read/write head position, the strain sensor output, the motion of the MA relative to the suspension tip displacement, respectively. In conventional single-stage disk drive systems, only y_h is available in the form of the PES by reading position information from servo sectors on the disk and comparing it with the desired head position. In dual-stage systems with a MEMS MA and an instrumented suspension, y_p and y_m are also measurable from the strain sensor on the suspension and the capacitive sensor embedded in the MA structure, respectively. In single-stage systems, y_v is equivalent to y_h since y_m is always zero; while in dual-stage systems, y_v is not directly measurable. However, it can be calculated by $y_v = y_h - y_m$.

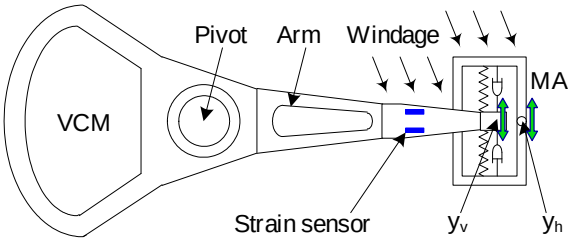

Figure 1: Schematic of the dual-stage system

Typically, the VCM/E-block/suspension assembly consists of a major bearing-friction mode, a butterfly mode, and a number of suspension resonance modes. Its transfer function from u_v to y_v can be expressed as

$$G_V(s) = \sum_{i=0}^{6} \frac{A_i}{s^2 + 2\zeta_i\omega_i s + \omega_i^2}\,, \tag{1}$$

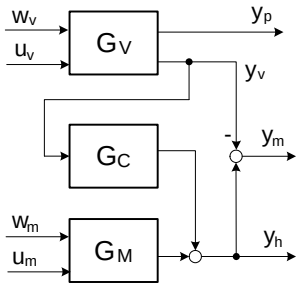

Figure 2: Block diagram of the dual-stage system

where for each mode i, A_i is the modal constant, ζ_i is the damping ratio, and ω_i is the natural frequency. Mode 0 denotes the bearing-friction mode around 100 Hz, the butterfly mode is around 7.4 kHz, and all other modes are suspension modes ranging from 5 kHz to 20 kHz, all with a light damping coefficient of about 0.015 N·s/m. Each suspension mode is excited by an independent windage source, and the strain sensor picks up vibration information from each mode with another set of values for A_i as those in Eq. (1).

The MA dynamics can be modelled as a second order system, and its transfer function from either u_m or w_m to y_h is

$$G_M(s) = \frac{A_m}{s^2 + 2\zeta_m\omega_m s + \omega_m^2}\,. \tag{2}$$

Usually the MA's natural frequency ω_m is designed to be between 1$\sim$2 kHz and ζ_m is about 0.1 N·s/m. G_C is the coupling dynamics from y_v to y_h. This is due to the fact that the translational motion of the slider/head, y_h, is excited by the suspension tip motion, y_v, through the MA's spring/damper structure. The coupling dynamics can be expressed as

$$G_C(s) = \frac{2\zeta_m\omega_m s + \omega_m^2}{s^2 + 2\zeta_m\omega_m s + \omega_m^2}\,. \tag{3}$$

Due to this coupling, y_m is the combined relative motion output from all the four inputs as shown in Fig. 2. On the other hand, the MA motion can be assumed to have little effect on the VCM/E-block/suspension dynamics due to the very small inertia of the MA compared to that of the VCM. This assumption means that the transfer function from u_m to y_v is constantly zero.

2.2 Disturbances Characterization

There are various kinds of disturbances entering the servo system of a disk drive. Many researches on disturbances characterization and suppression have been reported in the literature [11][12][13]. The disturbances entering the servo system can be roughly categorized into three types:

Torque disturbances, which include D/A quantization noise, power-amp noise, bearing imperfection and nonlinearity, and especially high-frequency airflow turbulence impinging on the suspension-slider assembly; *Track runout*, which includes nonrepeatable motion of the disk such as bearing imperfection and disk flutter, and repeatable track motion such as eccentricity due to disk slippage and imperfection of track circles due to written-in TMR; *Noises*, which include PES demodulation noise, sensor noises, and A/D quantization noise.

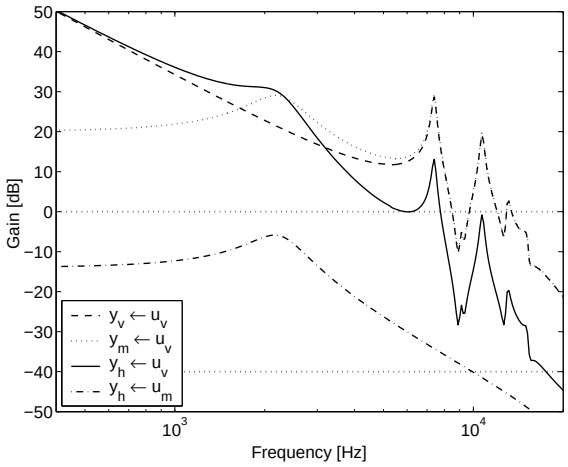

Figure 3: Frequency responses of the dual-stage actuator

In this paper, the disturbances are modelled as follows. The reference signal, r, includes track runout and the head motion resulting from all torque disturbances, except the airflow turbulence acting on the two actuators. A third order model is used to characterize its low frequency feature:

$$r(s) = \left(\frac{7.8 \times 10^9}{s^2 + 800s + 2.5 \times 10^5} + \frac{1.2 \times 10^5}{s + 1.9 \times 10^3} \right) w_r(s)\,, \tag{4}$$

where w_r is a normalized white noise. The RMS value of this runout is about 450 nm in the range of 10 Hz $\sim$ 25 kHz.

The airflow turbulence acting on the two actuators is respectively denoted as $\mathrm{w_v}$ and $\mathrm{w_m}$ for the design purpose of vibration suppression and compensation. Each suspension mode has an independent disturbance source which is assumed to be white. The airflow excited suspension vibration has an RMS value of about 5 nm, and the $\mathrm{w_m}$ excited MA vibration is about 4 nm. The three signals, y_p, y_m, and the PES, have their corresponding measurement noises. The three signals, PES, y_p and y_m, have their corresponding measurement noises with the RMS levels of 1 nm, 0.1 nm and 2 nm, respectively. These noise levels determine how heavily each signal can be utilized so that system performance can be optimized.

2.3 Multirate Sensing and Multirate Control

In conventional single-stage disk drives, the only feedback signal, PES:$= r - y_h$, has a fixed sampling rate that is predetermined by the disk rotation speed and the number of servo sectors per track. For example, a 7200-RPM disk drive with 180 servo sectors has a PES sampling frequency of 21.6 kHz. Given the disk rotation speed, a higher PES sampling frequency requires more servo sectors and reduces storage efficiency. This fixed sampling frequency limits the expected servo bandwidth which is about one tenth of this frequency. Further increase of servo bandwidth is also prevented by the presence of suspension resonance modes.

For a designed servo system, all disturbances below the closed-loop bandwidth can be attenuated to some extent. Those high-frequency disturbances, especially airflow excited suspension vibration, may be

Table 1: Parameter Variation

	A	ζ	ω
G_V	$\pm$5%	$\pm$20%	$\pm$ 8%
G_M	$\pm$5%	$\pm$20%	$\pm$12%

amplified according to the theorem of Bode's integral equality. Airflow excited suspension vibration has become a major obstacle to approaching the targeted track density of 500,000 TPI. However, with strain sensors instrumented on the suspension and with a secondary microactuator, high-frequency suspension vibration may be effectively suppressed and compensated by feeding the vibration information to the controller [14]. Furthermore, the sampling rate of the two signals can be higher than that of the PES for better performance. In some design schemes, the VCM and MA are intended to deal with the attenuation of low-frequency and high-frequency disturbances respectively, then u_v can be updated at a lower rate than that of u_m for computation saving [15]. A multirate sensing scheme can be carried out and a multirate controller is then accordingly designed.

In this paper, we assume that the PES has a sampling rate of 25 kHz, and both y_p and y_m are sampled at 50 kHz. For simplicity, both u_v and u_m are updated at the high rate of 50 kHz.

2.4 Plant Uncertainty

Plant uncertainty is inherent in all dynamic systems. Hard disk drives are typically fabricated in a huge batch, with each drive having slightly different dynamic response but the same nominal properties. When servo control is embedded in disk drive systems, it is infeasible to fine tune the controller parameters for each individual disk drive. Therefore the same control system should stabilize and perform well on all these disk drives. In this section, plant uncertainty is modelled for the dual-stage system so that robust stability can be explicitly considered in the controller design as follows.

2.4.1 Parametric Uncertainty

Since the dual-stage model is expressed as a combination of both suspension and MA modes, and each mode is defined by 3 parameters (i.e., A, ζ, ω), it is natural to consider this parametric uncertainty in both the controller design and its performance evaluation. In this paper, we assume that the variation range of each parameter with respect to its nominal value is as specified in Table 1. As well known, parametric uncertainty can be represented using linear fractional transformation (LFT) [16]. For example, suppose that there is a $\pm 10\%$ variation in parameter a, then the actual value a_a can be represented in terms of its nominal value a_n and that variation range using the following LFT

$$a_a = F_L \left(\begin{bmatrix} a_n & 0.1a_n \\ 1 & 0 \end{bmatrix}, \delta \right), \tag{5}$$

where F_L indicates that the lower loop of the matrix is closed with δ, and δ is a real-valued perturbation with $|\delta| \leq 1$.

Parametric uncertainty is a suitable model for performance evaluation due to its detailed characterization. However, since modelling parametric uncertainty usually results in a high dimension of the uncertainty Δ block, it is not so popularly used for controller design as dynamic uncertainty.

2.4.2 Multiplicative Dynamic Uncertainty

Multiplicative uncertainty can take into account not only unmodeled dynamics but also some effect of parametric uncertainty. A low dimensional Δ is therefore adequate for the design purpose. In the dual-stage actuator, two multiplicative uncertainties are assumed for the VCM and MA respectively:

$$\begin{aligned} G_V(s) &= G_{V\mathrm{nom}}(s)(1 + \Delta_V(s)W_V(s))\,, \\ G_M(s) &= G_{M\mathrm{nom}}(s)(1 + \Delta_M(s)W_M(s))\,, \end{aligned} \tag{6}$$

where, $G_{V\mathrm{nom}}$ and $G_{M\mathrm{nom}}$ are the nominal dynamics of the VCM and MA respectively, $||\Delta_V||_\infty \leq 1$, $||\Delta_M||_\infty \leq 1$, and W_V and W_M are the magnitude bounding functions of the two uncertainties:

$$\begin{aligned} W_V(s) &= 0.6\frac{s + 2\pi \times 400}{s + 2\pi \times 6000}\,, \\ W_M(s) &= 0.3\frac{s + 2\pi \times 1400}{s + 2\pi \times 10000}\,. \end{aligned} \tag{7}$$

2.4.3 Additive Uncertainty

Additive uncertainty can also be used to characterize some unmodelled dynamics, especially those in the high frequency range. It can be used along with parametric uncertainty in robust control design to better capture the uncertainty features. In this model, the additive uncertainties of G_V and G_M are assumed to be 0 dB (1.0) and -40 dB (0.01) respectively, as indicated by the two horizontal lines in Fig. 3. It is seen that with the additive uncertainties defined above, the VCM dynamics beyond 11 kHz and the MA dynamics beyond 10 kHz become highly inaccurate and hence unreliable.

2.5 A Generalized Plant with Multirate Sensing and Control

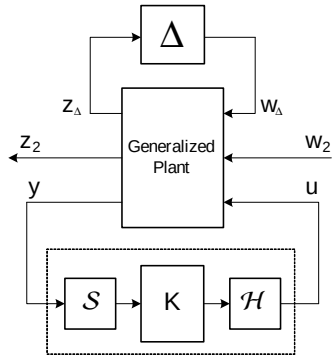

Figure 4: Multirate sensing and multirate control of the generalized plant

By combining all disturbance, measurement noise, and uncertainty models, we can obtain a generalized plant, which incorporates both multirate sensing and multirate control, as shown in Fig. 4. In the figure, Δ represents all types of normalized perturbations in a block-diagonal form. w_2 includes all types of normalized white disturbances. $z_2 := [\mathrm{PES}\, u_v\, u_m]^T$ is the weighted performance output. The weights on u_v and u_m are taken to be the reciprocals of their corresponding upper bounds, which are both 2 volts multiplied by the corresponding amplification gains of their conditioning circuits. $\mathcal{S}$ is the multirate sampler of the plant measurement output $y := [\mathrm{PES}\, y_p\, y_m]^T$. $\mathcal{H}$ is the multirate hold of the plant control input $u := [u_v\, u_m]^T$. Due to the multirate sampler $\mathcal{S}$ and hold $\mathcal{H}$, the controller K is also multirate, or equivalently, periodically time varying. The generalized plant has absorbed all frequency shaping filters and weights, in order to normalize these perturbations, disturbances, and performance outputs. Based on this generalized model, various design methods can be applied to design the controller K.

3 Robust Controller Design

Several controller design approaches have been proposed for dual-stage servo systems, which can be roughly categorized into two major groups. The first group includes those approaches that utilize sequential SISO design techniques, such as the PQ method [7], and the SD method [17][8]. The second group includes those MIMO optimal control design techniques such as μ-synthesis [9] and mixed H_2/H_∞ [6].

3.1 Sequential SISO Designs

In this section, two SISO design approaches are presented: the PQ design [7] and the SD design [8]. Both of these approaches will be augmented by a two-step design procedure: a high-rate inner loop damping controller is first implemented, followed by a low-rate track-following controller, which is design using a traditional sequential SISO technique. This approach to multi-rate and multi-variable control simplifies the controller design and facilitates the use of sequential SISO design techniques in the design process at the expense of constraining the controller structure, and hence only permitting suboptimal system performance.

3.1.1 Inner Loop Vibration Damping

When y_p and y_m are available as auxiliary information, it is feasible to first design inner loop vibration damping controllers before designing the outer loop tracking controller. As previously mentioned, the damping controllers are designed to run at a high rate to achieve better attenuation of airflow excited, high-frequency suspension vibrations.

The basic use of the relative motion signal, y_m, is to actively damp the MA resonance mode to make for a well-behaved MA and to simplify the control design that follows. This can be implemented as a minor loop around the MA as shown in the lower part of Fig. 5, where G_P is defined in Fig. 2. The two controllers, K_{MS} and K_{MR} are designed by solving a Diophantine equation with the desired closed-loop polynomial A_D. This polynomial is chosen by the designer based on the tradeoff between airflow excited vibration attenuation and measurement noise amplification [18].

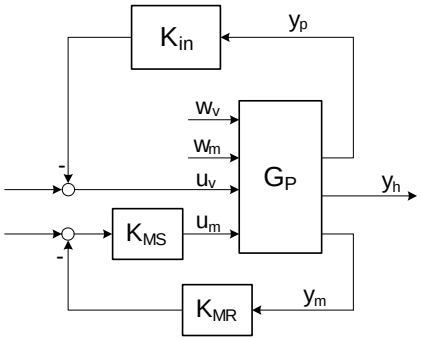

Figure 5: Minor loop vibration damping and compensation

After the minor loop around the MA is closed, a vibration controller K_{in} is designed using y_p to provide more damping for some of the suspension resonance modes. The design of K_{in} is formulated as a standard LQG problem, in which y_v is the output to be minimized and y_p is the measurement for feedback [19]. Fig. 6 shows the frequency responses of the open-loop plant and the damped plant as shown in Fig. 5. As can be seen, major resonance modes of the VCM/suspension assembly and the MA modes have been adequately damped.

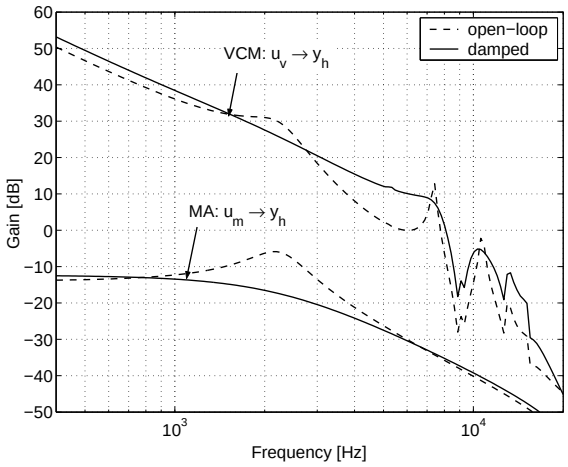

Figure 6: Comparison of frequency responses between open-loop plant and the damped plant

3.1.2 SD Design

The SD design approach has been popularly applied in the design of track-following controllers for dual-stage servo systems. This approach utilizes the PES and y_m to generate the position error of the suspension tip relative to the data track center, which will be labelled as VPES

$$\text{VPES} = \text{PES} + y_m = r - y_v \,. \tag{8}$$

This signal is then fed to the VCM loop controller K_V. This scheme is shown in Fig. 7(a), where G_{PD} is the damped plant as shown in Fig. 5. The closed-loop plant can further be reduced to two sequential loops,

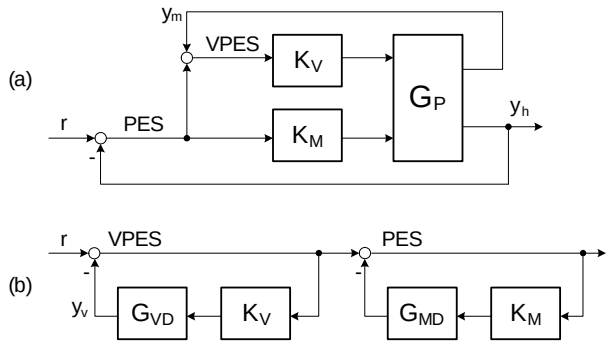

Figure 7: Sensitivity decoupling design

as shown in Fig. 7(b). The design of K_V and K_M now becomes straightforward: the VCM loop and the MA loop can be designed sequentially using conventional SISO design techniques, and the total sensitivity is the product of the two, as exemplified in Fig 8. The reader is referred to [20] for details of this method.

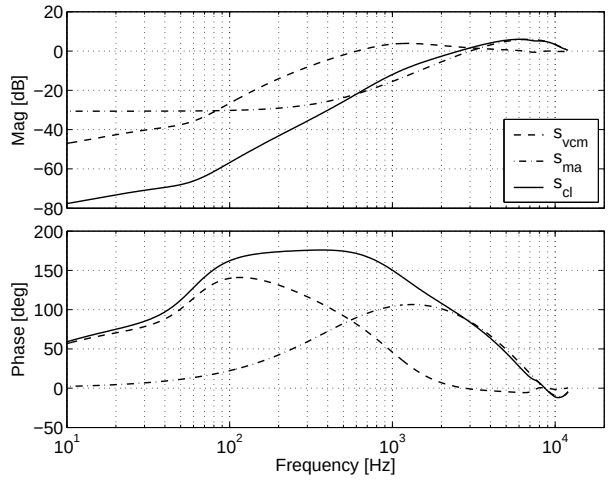

Figure 8: Sensitivities of the decoupling design

In order to compare the SD technique with other design approaches, the structure of the complete multirate controller, K in Fig. 5, for the SD technique is give by

$$K_{SD} = \begin{bmatrix} K_V & -K_{\text{in}} & K_V \\ K_{MS}K_M & 0 & -K_{MS}K_{MR} \end{bmatrix} \tag{9}$$

with inputs $[\text{PES}\,, \text{y}_\text{p}\,, \text{y}_\text{m}]^\text{T}$ and outputs $[u_v\,, u_m]^T$. From this we can clearly see the constraints that have been imposed on the controller structure for the ease of applying SISO design techniques. The second column is determined by the inner loop vibration damping using y_p, and the remaining two columns are determined by the outer loop controller.

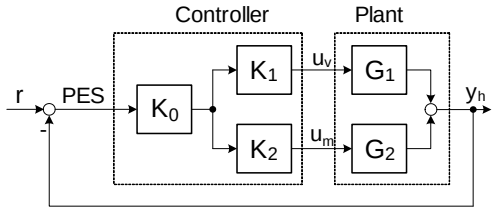

Figure 9: PQ design

3.1.3 PQ Design

The second design approach is called the PQ design [7], which reduces a control design problem for double-input single-output (DISO) systems into two sequential SISO designs. The first step of the PQ method addresses the issue of actuator interference as a function of frequency, and the second step allows the use of traditional loop shaping techniques to achieve the desired nominal system performance and adequate stability margin. Its scheme is illustrated in Fig. 9, where it is assumed that an inner loop damping, such as the one shown in Fig. 6, has already been implemented on both the VCM and MA.

To perform the PQ design, we first define

$$G_P(e^{j\omega}) := \frac{G_1(e^{j\omega})}{G_2(e^{j\omega})}\,, \tag{10}$$

which is the ratio between the two input-output channels of the plant as shown in Fig. 9. Subsequently, we design a compensator G_Q to stabilize the virtual plant G_P with unity feedback. The phase margin of the open-loop plant $G_P G_Q$ determines how much the outputs of the two actuators interfere around the handoff frequency. A large phase margin is pursued to ensure that the two actuators work cooperatively especially when the outputs of the two actuators are comparable in magnitude. The designed G_Q is then decomposed

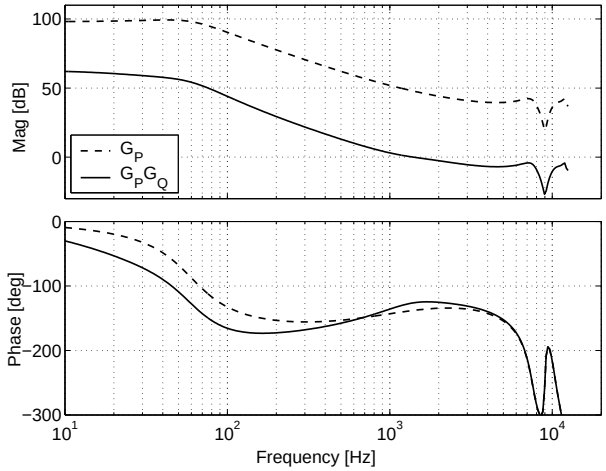

Figure 10: Frequency responses of G_P and G_{PQ}

into two parts with $G_Q = K_1/K_2$ such that both K_1 and K_2 are realizable. Finally a compensator K_0 is designed for the SISO plant

$$G_{\text{siso}} := K_1 G_1 + K_2 G_2\,, \tag{11}$$

using loop shaping techniques to achieve a desired gain crossover frequency and gain and phase margins.

The structure of the complete multirate controller, K in Fig. 5, for the PD design is given by

$$K_{PQ} = \begin{bmatrix} K_1 K_0 & -K_{\text{in}} & 0 \\ K_{MS} K_2 K_0 & 0 & -K_{MS} K_{MR} \end{bmatrix}. \tag{12}$$

Unlike the sensitivity decoupling design, the PQ method uses only the PES in the outer loop tracking controller. Hence the structure of K_{PQ} is even more constrained than K_{SD} in that the entry (1,3) is also zero.

3.2 MIMO Designs

By exploiting the coupling dynamics inherent in MIMO systems, MIMO robust design methods are expected to achieve better performance than their sequential SISO design counterparts, while still retaining robust stability. In this section, three multirate robust control design approaches are considered: mixed H_2/H_∞ [21], mixed H_2/μ, and robust H_2 synthesis [22].

3.2.1 Mixed H_2/H_∞ synthesis

This approach performs nominal H_2 minimization with several H_∞ bounds on channels from w_Δ to z_Δ, so that stability robustness can be explicitly taken into account during the design process. Since the H_∞ norm is usually not a precise measure for robust stability, especially when the uncertainty Δ block has a high dimension, only *multiplicative* uncertainties in the VCM and MA are considered in this design, which restrains the Δ block to a 2-by-2 diagonal matrix. Then the problem becomes

$$\min_K \gamma, \text{ subject to } \begin{cases} ||T_{z_2 w_2}(K)||_2 < \gamma, \\ ||T_{z_V w_V}(K)||_\infty < \gamma_V, \\ ||T_{z_M w_M}(K)||_\infty < \gamma_M, \end{cases} \tag{13}$$

where (z_V, w_V) and (z_M and w_M) are the I/O channels in the Δ block related to the VCM and MA respectively; γ_V and γ_M are bounds selected empirically so that $||T_{z_\Delta w_\Delta}(K)||_\infty < 1$ can finally be satisfied. The reader is referred to [21] for further details.

3.2.2 Mixed H_2/μ synthesis

Unlike mixed H_2/H_∞ synthesis, mixed H_2/μ synthesis minimizes the nominal H_2 norm with a μ (structured singular value) bound, since the μ bound is a precise measure for robust stability with both parametric and dynamic uncertainty [16]. The design procedure is similar to the D-K iteration in mu-synthesis with the alteration that the K part is designed by the mixed H_2/H_∞ optimization procedure rather than an H_∞ minimization. Therefore, the computation involves a series of optimization steps, and it can be solved via mixed H_2/H_∞ optimization with proper D-scaling:

$$\min_{K,D} \gamma, \text{ subject to } \begin{cases} ||T_{z_2 w_2}(K)||_2 < \gamma, \\ ||D T_{z_\Delta w_\Delta}(K) D^{-1}||_\infty < 1, \end{cases} \tag{14}$$

where the second inequality represents an upper bound of $\mu_\Delta(T_{z_\Delta w_\Delta}(K))$, which guarantees the robust stability of the closed-loop plant. The reader is referred to [16] for more details on μ analysis and synthesis. It is noted that the resulting controller order may be large due to the inclusion of dynamic D and D^{-1} matrices.

3.2.3 Robust H_2 synthesis

The previous two approaches can only optimize nominal performance rather than robust performance, and therefore, plant perturbation may degrade track-following performance to an unacceptable extent before the system becomes unstable. The third synthesis approach, robust H_2 synthesis, considers robust (or worst-case), rather than nominal, H_2 performance by taking into account *parametric* uncertainty during the design process. This is achieved by solving

$$\min_K \max_\Delta ||T_{z_2 w_2}(K, \Delta)||_2 \,. \tag{15}$$

If $T_{z_2 w_2}(K, \Delta)$ is affine in Δ, this problem can be solved by an optimization that solves a set of matrix inequalities with respect to all vertices of the polyhedron formed by all parametric uncertainties. Since the two decision variables in the matrix inequalities are coupled, which makes the inequalities nonconvex, an iteration process is executed to make the optimization step-wise convex by fixing one variable at each step. This procedure is also similar to the D-K iteration process in μ synthesis, and the reader is referred to [23] for more details. The size of the involved optimization problem increases exponentially as the number of uncertain parameters increases, and therefore, only a few parametric uncertaities can be considered in the design.

Some comments can be made on the three MIMO design approaches. First, all of the three approaches reformulate the multi-objective design problem into the optimization of a set of linear matrix inequalities (LMIs), and therefore the designed controllers rely on numerically efficient convex optimization solvers like SeDuMi [24]. Second, the multirate aspect of the problem can be accounted for as follows. An augmented low-rate time-invariant system is constructed from the original high-rate time-varying system with a so-called Z-shifting matrix, which contains the periodicity information of the original system. Then designing a periodically time-varying controller for the original system is equivalent to designing a time-invariant controller for the auxiliary system. A set of periodically time-varying controllers is then designed all at once, with each controller being executed at a certain time instant within a period. The reader is referred to [22] for more details of the procedure. Third, in accordance with the multirate control design, balanced truncation can be performed on the periodically time-varying full-order controller [25], in order to get a reduced-order controller, which is necessary for practical implementation.

4 Design and Simulation Results

In all sequential SISO and MIMO design techniques, the actual controller design was performed on a simplified plant model, which includes three major VCM/E-block/suspension assembly modes and one MA reso-

Table 2: Performance comparison between control designs

Unstable cases are counted based on 400 perturbed plants. 'Degradation" denotes the ratio of worst-case over nominal performance. The 3-element vectors for robust H_2 indicate the availability of the three outputs [PES y_p y_m].

Design Approach	Unstable (/400)	PES (nm)			u_m (mV)			Controller Order
		Nominal	W-C	Degradation	Nominal	W-C	Degradation	
PQ method	0	7.75	10.00	129 %	205	234	114 %	6
SD method	0	7.11	8.35	117 %	277	316	114 %	6
Mixed H_2/H_∞	0	6.57	7.82	119 %	201	216	108 %	8
Mixed H_2/μ	0	5.31	5.88	111 %	261	298	114 %	8
Robust H_2 [1 1 1]	0	5.93	6.47	109 %	275	310	113 %	9
Robust H_2 [1 0 1]	0	5.96	7.10	118 %	308	388	126 %	10
Robust H_2 [1 1 0]	0	6.09	7.97	131 %	239	309	129 %	10
Robust H_2 [1 0 0]	0	7.66	9.45	123 %	278	399	144 %	10

nance mode. However, the full-order plant model, which includes seven VCM-suspension assembly modes and the MA mode, was used in the evaluation and comparison of the designed controllers and closed-loop systems.

Three criteria are checked on the full-order closed-loop systems: robust stability, nominal performance, and worst-case performance. The designed controller should robustly stabilize actual plants with bounded parametric variations as defined in Table. 1. Here, 400 plant samples are formed by randomly choosing a set of parameters from within their respective variation ranges. Unstable cases are then counted from the closed-loop systems. If all of these closed-loop systems are stable, then the worst-case performance can also be obtained. Here, two performance terms are considered: the RMS values of the PES and the control effort u_m. The magnitude of y_m is indirectly constrained by minimizing u_m so that it does not exceed the MA stroke. The VCM input u_v is usually very small compared to its range in the track-following mode. The simulation results are listed in Table 2. In that table, each robust H_2 result is labelled by a 3-element vector indicating the availability of the three outputs $[\mathrm{PES}\, y_p\, y_m]$. A value of 1 means that the corresponding signal was used in the control structure, while a 0 indicates that the signal was not used. "Degradation" is computed for the worst-case performance with respect to the nominal performance. Model reduction has been performed before obtaining the final controllers.

Several comparisons can be made between the various design approaches and the following conclusions can be drawn from them.

1) Robust Stability: All of the five design methodologies yielded closed-loop systems that are robustly stable under the assumed parametric uncertainty model defined in Table 1. For the two SISO techniques, robustness to mode variation is mainly achieved through the incorporation of the inner loop damping of

the VCM and MA. For the MIMO designs, stability robustness is incorporated in the MIMO controllers by imposing auxiliary H_∞ norm or μ bounds, or by considering parametric uncertainty directly.

2) SISO designs: As for the two SISO design approaches, the SD method achieves better performance than that of the PQ method, because the relative MA motion, y_m, is utilized in the design of the outer loop tracking controller for the SD design but not for the PQ design. However, the variance of u_m is much smaller in the PQ method than in the SD method. This is probably due to the fact that the PQ design methodology explicitly takes actuator interference into account.

3) MIMO designs: The mixed H_2/μ approach achieved the best nominal and worst-case performance of all three MIMO techniques. This is attributed to the precise characterization of robust stability criterion through μ, which makes the controller less conservative and its capability can hence be fully exploited. The robust H_2 design achieves moderate performance with the smallest performance degradation. This is mainly due to the explicit consideration of worst-case performance during the design process. Both of the two methods yielded controllers that perform better than the mixed H_2/H_∞ design, indicating the conservativeness introduced by the H_∞ norm bounds for achieving robust stability.

4) SISO design vs. MIMO design: It can be clearly seen that the MIMO designs always perform better than their sequential SISO counterparts, not only with respect to nominal performance, but also with respect to worst-case performance. Performance degradation due to parameter variations from nominal values also shows the same trend: it increases at a smaller rate for MIMO designs than for SISO designs. These results show that MIMO designs are more aggressive in optimizing system performance by better exploiting the coupling property of the MIMO system while still guaranteeing robust stability.

It is also observed that the control input effort at the MA, u_m, is not necessarily larger in MIMO designs than in SISO designs. This implies that MIMO designs achieve small tracking error by optimizing their controllers rather than by putting more control effort into the system.

5) Multi-sensing: The effect of multi-sensing is also checked by comparing different sensing schemes. A comparison of the four cases of robust H_2 shows that the use of either y_m and y_p can improve system performance significantly, while using both signals can achieve the best nominal performance with the smallest performance degradation. The use of the relative position measurement y_m makes the MA more robust to its mode uncertainty, and also makes it possible to optimally distribute the control effort between the VCM and MA. However, a dedicated vibration sensor can provide suspension vibration information at a higher signal-to-noise ratio and hence is necessary during approaching the extremely stringent target, 500k TPI. Improvement by multi-sensing is also due to the fact that y_p and y_m are sampled at a higher rate than that of the PES. With only the PES available at the low rate, we see significant performance degradation compared to the three multi-sensing cases.

6) Controller order: Controller order reduction was conducted on all three MIMO controllers, so that they can be implemented on the DSP board. However, care must be taken during implementation. Since these controllers are MIMO and dynamically coupled, they may be more sensitive to quantization error than their sequential SISO counterparts. It should also be noted that these MIMO controllers are periodically time-varying, which means that a set of controllers are designed and the set of parameter values for each

time-varying controller must be stored and retrieved. As a consequence, more memory is needed for storing the time varying parameters, in order to implement these controllers.

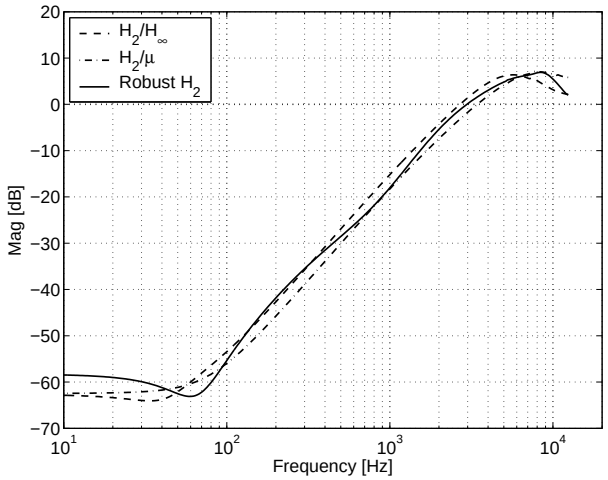

Figure 11: Frequency responses of the sensitivity transfer functions from the three MIMO designs

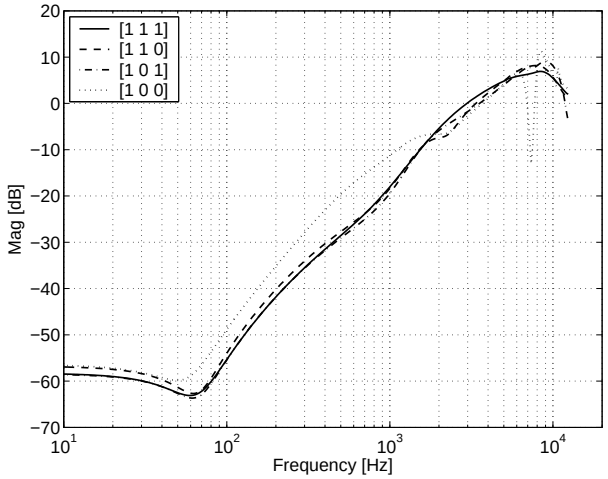

Figure 12: Comparison of different sensing schemes with the robust H_2 design approach

Fig. 11 shows the frequency responses of the nominal sensitivity transfer functions by the three MIMO design approaches: mixed H_2/H_∞, mixed H_2/μ and robust H_2. The sensitivity transfer function is defined from the reference input, or equivalently track runout, to the PES. These responses have almost the same peak gains with different closed-loop bandwidth. Higher bandwidth usually implies stronger attenuation in the low frequency range. So, the mixed H_2/μ design performs best and the robust H_2 design is better than the mixed H_2/H_∞ one. Fig. 12 shows the frequency responses of the nominal sensitivity functions of robust H_2 design with different sensing schemes. The first three systems have similar sensitivity responses, but with different worst-case performance as shown in Table 2. The last system with only the PES measurable has the worst error attenuation below its bandwidth, also there are drastic fluctuations beyond its bandwidth, implying bad performance robustness. All these observations are consistent with those conclusions drawn

from Table 2.

5 Conclusion

In this paper, we have presented the system modelling, design, and comparison of several multirate robust track-following controllers for a dual-stage servo system that utilizes a MEMS microactuator and an instrumented suspension. A complete plant model, including nominal dynamics, sensing schemes, disturbances, and plant uncertainties, was developed. Two SISO design approaches, the PQ design and the SD design, and three multirate robust MIMO design approaches, mixed H_2/H_∞, mixed H_2/μ and robust H_2 synthesis, were considered.

Design and simulation results showed that the robust MIMO design approaches generally achieve better nominal and worst-case performance than their sequential SISO design approach counterparts. These advantages were achieved by optimizing the H_2 performance of the control system, while considering robust stability explicitly, and also by making the controller multirate in a strict sense. On the other hand, the SISO design approaches are straightforward to use and easy to implement.

The integration of a dual-stage actuator equipped with a MEMS translational microactuator and an instrumented suspension is currently in progress in our research lab. Experimental verification will be conducted once the complete system is available.

References

[1] HGST, "Perpendicular recording," http://www.hitachigst.com/hdd/research/recording_head/pr/index.html, 2005.

[2] T. Hirano, M. White, H. Yang, K. Scott, S. Pattanaik, S. Arya, and F.-Y. Huang, "A moving-slider mems actuator for high-bandwidth hdd tracking," in *Proc. Intermag*, vol. 3, 2003, pp. 2535–2540.

[3] K. Oldham, S. Kon, and R. Horowitz, "Fabrication and optimal strain sensor placement in an instrumented disk drive suspension for vibration suppression," in *Proc. Amer. Control Conf.*, 2004, pp. 1855–1860.

[4] Y. Huang, M. Banther, P. D. Mathur, and W. Messner, "Design and analysis of a high bandwidth disk drive servo system using an instrumeted suspension," *IEEE/ASME Trans. Mechatronics*, vol. 4, no. 2, pp. 196–206, 1999.

[5] Y. Li and R. Horowitz, "Active vibration control of a pzt actuated suspension in hard disk drives," in *Proc. Amer. Control Conf.*, May 2002, pp. 1366–1371.

[6] X. Huang, R. Nagamune, R. Horowitz, and Y. Li, "Design and analysis of a dual-stage disk drive servo system using an instrumented suspension," in *Proc. Amer. Control Conf.*, 2004, pp. 535–540.

[7] S. J. Schroeck and W. C. Messner, "On controller design for linear time-invariant dual-input single-output systems," in *Proc. Amer. Control Conf.*, San Diego, CA, June 1999, pp. 4122–4126.

[8] Y. Li and R. Horowitz, "Mechatronics of electrostatic microactuators for computer disk drive dual-stage servo systems," *IEEE/ASME Trans. Mechatronics*, vol. 6, no. 2, pp. 111–121, 2001.

[9] D. Hernandez, S.-S. Park, R. Horowitz, and A. K. Packard, "Dual-stage track-following servo design for hard disk derives," in *Proc. Amer. Control Conf.*, San Diego, CA, June 1999, pp. 4188–4121.

[10] G. E. Dullerud and S. Lall, "A new approach for analysis and synthesis of time-varying systems," *IEEE Trans. Automat. Control*, vol. 44, no. 8, pp. 1486–1497, 1999.

[11] R. Ehrlich and D. Curran, "Major HDD TMR sources and projected scaling with TPI," *IEEE Trans. Magnetics*, vol. 35, no. 2, pp. 885–891, 1999.

[12] L. Guo, H. S. Lee, A. Hudson, and S.-H. Chen, "A comprehensive time-domain simulation for HDD TPI prediction and mechanical/servo enhancement," *IEEE Trans. Magnetics*, vol. 35, pp. 879–884, 1999.

[13] L. Guo and Y.-J. D. Chen, "Disk flutter and its impact on HDD servo performance," *IEEE Trans. Magnetics*, vol. 37, no. 2, pp. 866–870, 2001.

[14] Y. Li, F. Marcassa, R. Horowitz, R. Oboe, and R. Evans, "Track-following control with active vibration damping of a PZT-actuated suspension dual-stage servo system," in *Proc. Amer. Control Conf.*, 2003, pp. 2553–2559.

[15] S.-C. Wu and M. Tomizuka, "Performance and aliasing analysis of multirate digital controllers with interlacing," in *Proc. Amer. Control Conf.*, 2004, pp. 3154–3159.

[16] G. J. Balas, J. C. Doyle, K. Glover, A. Packard, and R. Smith, *μ-Analysis and Synthesis Toolbox for use with MATLAB*. MUSYN Inc. and The MathWorks, Inc., USA, 1995.

[17] K. Mori, T. Munemoto, H. Otsuki, Y. Yamaguchi, and K. Akagi, "A dual-stage magnetic disk drive actuator using a piezoelectric device for a high track density," *IEEE Trans. Magnetics*, vol. 27, no. 6, pp. 5298–5300, Nov. 1991.

[18] M. T. White and T. Hirano, "Use of relative position signal for microactuators in hard disk drives," in *Proc. Amer. Control Conf.*, 2003, pp. 2535–2540.

[19] Y. Li, R. Horowitz, and R. Evans, "Vibration control of a pzt actuated suspension dual-stage servo system using a pzt sensor," *IEEE Trans. Magnetics*, vol. 39, no. 2, pp. 932–937, 2003.

[20] Y. Li and R. Horowitz, "Active suspension vibration control with dual-stage actuators in hard disk drives," in *Proc. Amer. Control Conf.*, June 2001, pp. 2786–2791.

[21] X. Huang and R. Horowitz, “Robust controller design of a dual-stage disk drive servo system with an instrumented suspension,” *IEEE Trans. Magnetics*, vol. 8, no. 5, pp. 194–200, August 2005.

[22] R. Nagamune, X. Huang, and R. Horowitz, “Multirate track-following control with robust stability for a dual-stage multi-sensing servo system in hdds,” in *Proc. IEEE Conf. Decision and Control*, Dec. 2005.

[23] ——, “Multirate robust track-following control for dual-stage multi-sensing servo systems in hdds: Part II,” *IEEE Trans. Control System Technology*, Under preparation.

[24] J. F. Sturm, *Using Sedumi 1.05, A MATLAB Toolbox for Optimization over Symmetric Cones*, 2001.

[25] A. Varga, “Balanced truncation model reduction of periodic systems,” in *Proc. 38th Conf. on Decision and Control*, 2000, pp. 2379–2384.